IEEE Access
Multidisciplinary | Rapid Review | Open Access Journal

Received August 10, 2017, accepted September 15, 2017, date of publication September 20, 2017,
date of current version October 12, 2017.

Digital Object Identifier 10.1109/ACCESS.2017.2754521

Analysis of a Whole-Space Transient Electromagnetic Field in 2.5-Dimensional FDTD Geoelectric Modeling

ZHIHAI JIANG[1], SHUCAI LIU[1], AND REZA MALEKIAN[2], (Senior Member, IEEE)
[1]Department of Applied Geophysics, China University of Mining and Technology, Xuzhou, 221116 China
[2]Department of Electrical, Electronic and Computer Engineering, University of Pretoria, Pretoria 0002, South Africa

Corresponding author: Shucai Liu (liushucai@cumt.edu.cn)

This work was supported in part by the Major State Basic Research Development Program of China(973 Program) under Grant 2013CB227900, in part by the National Natural Science Foundation of China under Grant 41304113, in part by the China Scholarship Council under Grant 201606425004, and in part by the National Research Foundation, South Africa under Grant IFR160118156967 and Grant RDYR160404161474.

ABSTRACT Mine water inrush poses a serious threat to the safe production of coal mines in China. The transient electromagnetic method (TEM) on the ground has been applied to explore water-bearing structures, but the resolution is low. Therefore, some geophysicists in China moved the TEM onto underground coal mine roadways and obtained good results at the end of the last century. Although the TEM has been applied in mining for many years, there are so few theoretical studies that the data interpretation is not accurate. It is necessary to study the transient electromagnetic field diffusion in the entire space with physical or numerical simulation methods. First, based on the diffusion equations, we deduced the wave number domain equations, whose whole-space electromagnetic field is excited by a 3-D source in a 2-D geoelectric model; then, we derived the 2.5-D finite-difference time domain equations. At the beginning of the calculation, we gave the grid nodes near the source the initial values with the cosine filtering method. To improve the calculating efficiency, the time intervals gradually increased with time. At the end of the calculation, we transformed the calculating results from the wave number domain to the space domain by fitting the segmented exponential function. Compared with the analytical solutions, the numerical solutions are accurate, and the algorithm is reliable and efficient. The simulation results of a collapse-column model show that the transient electromagnetic field diffusion in the entire space is dominated by low-resistivity bodies.

INDEX TERMS Finite-difference time domain method, geoelectric model, transient electromagnetic field, wave number domain, whole-space.

I. INTRODUCTION

Water inrush hazards have seriously affected the safe production of coal mines in China. With the increase in mining depth and excavation intensity, this problem is becoming increasingly serious. Geophysical methods are used to detect water-bearing structures before mining and have been one of the main technical means of mine water disaster prevention in China [1]. The transient electromagnetic method (TEM) on the ground, which is sensitive to low-resistivity bodies, has been widely applied in the hydrogeological investigation of coal mines [2]. However, it is difficult to obtain good results when the topography is complicated or when there are many humanistic facilities near the observing station. Far from the target body, the response signal is weak, and the resolution is low. In other words, the TEM on the ground cannot satisfy the high-precision requirements of coal mines to detect the water-bearing structures. To improve the signal strength and resolution, some geophysicists moved the TEM to the underground roadways of coal mines with a small multi-turn loop and obtained good results in detecting water-bearing bodies [3]–[5]. Meanwhile, to quickly and effectively detect the water-bearing structure in front of a tunnel wall, the TEM was introduced into tunnel condition work [6], [7]. For higher resolution on the distributions and shapes of low-resistivity bodies such as karst water and karst pipes, reference [8] developed a multi-component and multi-array TEM, which

can be applied in tunneling and defined the expressions of apparent resistivity. To improve the interpretation accuracy of TEM in mines and tunnels, the studies mainly focused on the time-depth transformation [9], apparent resistivity calculation [10], [11] and imagination [12]–[14].

When we apply TEM in the underground, the transient electromagnetic field diffuses in the entire space and the received response signal are affected by the medium in the entire space, which is different from the field of TEM on the ground. Thus, it is necessary to study the response characteristics of the transient electromagnetic field in the entire space. Reference [15] developed a computer code that computed the whole-space transient electromagnetic field for a horizontal square loop in a layered earth; the simulation results show that the vertical magnetic field is identical when the conductive layer is located either above or below the measurement station, but the horizontal magnetic field depends on the vertical position of the conductive layer, its conductivity, thickness and distance. Reference [16] and [17] developed a 3D finite-difference time domain program to simulate the whole-space response characteristics of a three-dimensional conductive body below the mine drift. Reference [18] proposed a numerical simulation method to design geosteering tools Reference [19] presented a finite-difference time-domain approach to simulate the three-dimensional transient electromagnetic diffusion phenomena to detect water-bearing structures in front of a tunnel face.

The two-dimensional model is closer to the actual geological structures than the one-dimensional model. The two-dimensional algorithm is simpler and easier to program than the three-dimensional one. Moreover, the calculation speed of the 2D algorithm is fast. In this paper, to study the response characteristics of the whole-space transient electromagnetic field in coal mines, we proposed a 2.5D finite-difference time domain (FDTD) to simulate the whole-space transient electromagnetic field. First, we deduced the wave number domain equations. Then, we calculated the whole-space electromagnetic field excited by a magnetic dipole in the wave number domain. Finally, we used a digital filter method to do the inverse Fourier transform and obtained the desired results.

II. 2.5D TIME DOMAIN FINITE-DIFFERENCE EQUATION

The passive diffusion equations for the electromagnetic field are [20]

$$\nabla^2\mathbf{E} - \mu\sigma\left(\partial\mathbf{E}/\partial t\right) = 0 \tag{1}$$

$$\nabla^2\mathbf{H} - \mu\sigma\left(\partial\mathbf{H}/\partial t\right) = 0 \tag{2}$$

where $\mathbf{E}$ is the electric field intensity, $\mathbf{H}$ is the magnetic field intensity, μ is the magnetic permeability, σ is the conductivity of the medium, and t is the time. To achieve a 2.5D numerical solution of (1) and (2), the key is to perform the Fourier transform in the direction of y and transform (1) and (2) into equations in a wave number domain. The transforming equation is

$$\hat{H}\left(x,\lambda,z\right) = \int_{-\infty}^{\infty} H\left(x,y,z\right)\exp\left(-i\lambda y\right)dy \tag{3}$$

where $\hat{H}$ is the magnetic permeability in the wave number domain, and λ is the wave number. Using the differential characteristics of the Fourier transform, we obtain

$$\nabla\hat{\mathbf{H}} = \left(\partial\hat{H}/\partial x\right)\mathbf{u}_x + i\lambda\hat{H}\mathbf{u}_y + \left(\partial\hat{H}/\partial z\right)\mathbf{u}_z \tag{4}$$

where $\mathbf{u}_x$, $\mathbf{u}_y$, and $\mathbf{u}_z$ are the unit vectors in the directions of x, y and z, respectively. Because the conductivity is homogeneous in the y direction for the 2D medium, the field component equations in the wave number domain can be derived from equations (1)-(4) (here n: x, y, z)

$$\partial^2\hat{E}_n/\partial x^2 + \partial^2\hat{E}_n/\partial z^2 - \lambda^2\hat{E}_n = \mu\sigma\left(\partial\hat{E}_n/\partial t\right)$$
$$\partial^2\hat{H}_n/\partial x^2 + \partial^2\hat{H}_n/\partial z^2 - \lambda^2\hat{H}_n = \mu\sigma\left(\partial\hat{H}_n/\partial t\right)$$

For simplicity, all field components are denoted by h. The equation for the wave number domain is

$$\partial^2 h/\partial x^2 + \partial^2 h/\partial z^2 - \lambda^2 h = \mu\sigma\left(\partial h/\partial t\right) \tag{5}$$

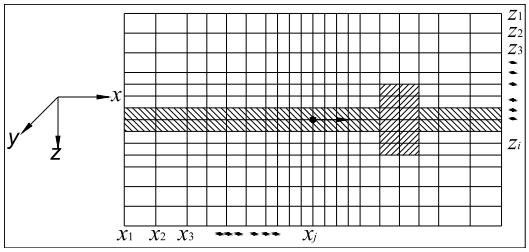

FIGURE 1. Whole-space FDTD mesh.

Figure 1 is the whole-space finite difference grids, Figure 2 shows a typical node and adjacent nodes in Figure 1. The coordinates of node (i, j) are x_i and z_i. h is the field value in the wave number domain, (5) is integrated along the ABCD rectangle, which is formed by four midpoints of 4 adjacent rectangles.

With Green's theorem, we obtain

$$\begin{aligned}\iint_{ABCD}\mu\sigma\left(\partial h/\partial t\right)dxdz &= \iint_{ABCD}\left(\partial^2 h/\partial x^2 + \partial^2 h/\partial z^2 - \lambda^2 h\right)dxdz \\ &= \int_{BC}\partial h/\partial z dx - \int_{AD}\partial h/\partial z dx + \int_{DC}\partial h/\partial x dz \\ &\quad - \int_{AB}\partial h/\partial x dz - \iint_{ABCD}\lambda^2 h dxdz\end{aligned} \tag{6}$$

Approximate transformation is performed on all integrations of the above formula and rearranged to obtain

$$\begin{aligned}\left(\mu\overline{\sigma}_{i,j}/2\right)\cdot\left(\partial h_{i,j}/\partial t\right) &= A_1 h_{i-1,j} + A_2 h_{i+1,j} \\ &\quad + A_3 h_{i,j-1} + A_4 h_{i,j+1} + A_5 h_{i,j}\end{aligned} \tag{7}$$

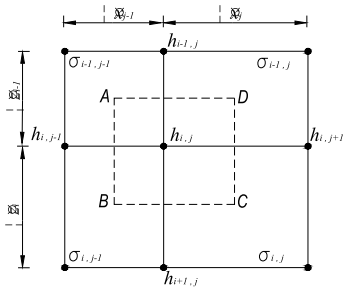

FIGURE 2. Grid nodes.

Here, the value of $\overline{\sigma}_{i,j}$ is given in the equation shown at the bottom of this page.

To discretize the diffusion equation, we must also approximate the time derivative of the equation. The approximation solution of the time derivative of the wave number domain equations is identical to the normal. For this model with the same space interval $\Delta x = \Delta z = \Delta$, (7) becomes

$$\partial h^n_{i,j}/\partial t = \left(h^n_{i-1,j} + h^n_{i+1,j} + h^n_{i,j-1} + h^n_{i,j+1} - 4h^n_{i,j} - \Delta^2\lambda^2 h^n_{i,j}\right) /\mu\overline{\sigma}_{i,j}\Delta^2 \tag{8}$$

Here, $\partial h^n_{i,j}/\partial t$ is the field at time $t = n\Delta t$.

The simplest approximation of the time derivative is the forward difference between the time of $t = n\Delta t$ and $t = (n+1)\Delta t$, namely,

$$\partial h^n_{i,j}/\partial t \approx \left(h^{n+1}_{i,j} - h^n_{i,j}\right)/\Delta t \tag{9}$$

This formula is accurate to the first approximation of Δt. Substituting (9) into (8), we obtain $h^{n+1}_{i,j}$, which is the forward difference expression of the diffusion equation in time:

$$h^{n+1}_{i,j} = \left[1 - \left(4 + \Delta^2\lambda^2\right) r_{i,j}\right] h^n_{i,j} + r_{i,j}\left(h^n_{i+1,j} + h^n_{i-1,j} + h^n_{i,j+1} + h^n_{i,j-1}\right) \tag{10}$$

In this formula,

$$r_{i,j} = \Delta t/\left(\mu\overline{\sigma}_{i,j}\Delta^2\right)$$

is dimensionless and named the local grid degree.

According to the results [21] proven by Oristaglio and Hohmann, in the wavenumber domain, to maintain the stability of inhomogeneous model problems, $r_{i,j}$ should not exceed $1/(4 + \Delta^2\lambda^2)$. Thus, the maximum time interval of (10) is

$$\Delta t_{max} = \mu min\left(\overline{\sigma}_{i,j}\right)\Delta^2/\left(4 + \Delta^2\lambda^2\right) \tag{11}$$

Here, $\min(\bar{\sigma}_{i,j})$ is the smallest value of $\bar{\sigma}_{i,j}$ in the model.

To increase the space and time interval and to reduce the difficulty of program design, we used the explicit unconditionally stable central difference approximation of the diffusion equation. For a non-uniform grid, the recursive discrete central difference approximation formula is

$$\partial h^n_{i,j}/\partial t \approx \left(h^{n+1}_{i,j} - h^{n-1}_{i,j}\right)/2\Delta t \tag{12}$$

$$h^n_{i,j} \approx \left(h^{n+1}_{i,j} + h^{n-1}_{i,j}\right)/2 \tag{13}$$

Substituting (13) into (9), we obtain the non-uniform grid central difference approximation equation:

$$h^{n+1}_{i,j} = 4\Delta t/\left(\mu\overline{\sigma}_{i,j} - 2\Delta t A_5\right) \cdot \left(A_1 h^n_{i-1,j} + A_2 h^n_{i+1,j} + A_3 h^n_{i,j-1} + A_4 h^n_{i,j+1}\right) + \left(\mu\overline{\sigma}_{i,j} + 2\Delta t A_5\right)\cdot h^{n-1}_{i,j}/\left(\mu\overline{\sigma}_{i,j} - 2\Delta t A_5\right) \tag{14}$$

In the two-dimensional wave number domain, the solution is obtained in the following steps: At any $n\Delta t$ time (n is an odd number), h^{n-1}_{ij} ($i+j$ is an odd number) can be projected to the $(n+1)$ level with the differential equation (14); then, h^n_{ij} ($i+j$ is an even number) can be projected to the $(n+2)$ level with the calculated solution, and so on. The two values of the field at moments $n = 0$ and $n = 1$ are given at the beginning of the computation, and the value of these fields are obtained through the whole-space homogeneous analytical solution.

III. INITIAL VALUE SEEKING

A. EXCITATION SOURCE

According to the above discussion, using the recursive calculation of the central difference method, we must calculate the initial value of the transient electromagnetic field at each node at the initial moments t_1 and t_2. Because the time is notably early at the initial two moments, the propagation region of the secondary field is notably small and concentrated near the excitation source. The region near the excitation source can be equivalent to the uniform space, so the field value can be obtained from the analytical solution of the uniform whole space at the two initial moments. The second field is excited by the beginning of the step pulse in the theoretical

$$\overline{\sigma}_{i,j} = \frac{\sigma_{i-1,j-1}\Delta z_{i-1}\Delta x_{j-1} + \sigma_{i,j-1}\Delta z_i\Delta x_{j-1} + \sigma_{i-1,j}\Delta z_{i-1}\Delta x_j + \sigma_{i,j}\Delta z_i\Delta x_j}{\left(\Delta z_{i-1} + \Delta z_i\right)\left(\Delta x_{j-1} + \Delta x_j\right)}$$

$$A_1 = 1/\left[\Delta z_{i-1}\left(\Delta z_{i-1} + \Delta z_i\right)\right]$$

$$A_2 = 1/\left[\Delta z_i\left(\Delta z_{i-1} + \Delta z_i\right)\right]$$

$$A_3 = 1/\left[\Delta x_{j-1}\left(\Delta x_{j-1} + \Delta x_j\right)\right]$$

$$A_4 = 1/\left[\Delta x_j\left(\Delta x_{j-1} + \Delta x_j\right)\right]$$

$$A_5 = -\left[1/\left(\Delta z_i\Delta z_{i+1}\right) + 1/\left(\Delta x_j\Delta x_{j+1}\right) + \lambda^2/2\right]$$

analysis, which we also performed in the paper. When the transmitting current ring is on the y-z plane in the Cartesian coordinate system, the transient magnetic field generated by the magnetic dipole, which is the input step pulse current, is [22] as follows:

$$\mathbf{E}_z = \mu m\theta^3 y \cdot \exp(-\theta^2 r^2) \cdot \mathbf{u}_z / \left(2\pi^{3/2} t\right) \tag{15}$$

$$\mathbf{E}_y = -\mu m\theta^3 z \cdot \exp(-\theta^2 r^2) \cdot \mathbf{u}_y / \left(2\pi^{3/2} t\right) \tag{16}$$

where m is the magnetic moment. The electric field only has components in the y and z directions, and the total electric field value is $E = \left(E_z^2 + E_y^2\right)^{1/2}$.

The time derivative of the transient magnetic field generated by the magnetic dipole is

$$\begin{aligned} \partial \mathbf{H}/\partial t &= m\theta^3 \exp\left(-\theta^2 r^2\right) / \left(\pi^{3/2} t\right) \\ &\cdot [\theta^2 r^2 \left(x^2 \mathbf{u}_x / r^2 + yz\mathbf{u}_y / r^2 + xz\mathbf{u}_z / r^2\right) \\ &+ \left(1 - \theta^2 r^2\right) \mathbf{u}_x] \end{aligned} \tag{17}$$

here, θ is the function defined to solve the step response

$$\begin{aligned} \theta &= [\mu\sigma / (4t)]^{1/2} \\ erfc(\theta r) &= 1 - erf(\theta r) \\ &= 1 - \left(2/\pi^{1/2}\right) \int_0^{\theta r} \exp\left(-\nu^2\right) d\nu \end{aligned}$$

Based on previous research, although the value of the transient electromagnetic field generated by the beginning of the step pulse is different from that generated by the end of the step pulse, the time derivative of the transient electromagnetic field has the same magnitude in the opposite direction [23]. However, the selection of the initial time and given initial node is notably important for the accuracy of the algorithm. If the initial moment is selected earlier, the initial number of nodes may be smaller; if the initial moment is later, the initial number of nodes should be increased. In this calculation process, we may select the initial moments earlier according to the following experiential formula:

$$t_0 = 1.13\mu\sigma\Delta_{min}^2$$

Here, μ is the permeability of the surrounding rock; σ is the conductivity; and Δ_{min} is the minimum space interval.

B. GIVING INITIAL VALUES

Equation (17) is an analytical formula in the spatial domain. Fourier transform on the source is made in the y direction for the difference in the wave number domain. Its Fourier transform formula is

$$h(x, k, z, t) = \int_{-\infty}^{+\infty} H(x, y, z, t) \exp(-iky)\, dy \tag{18}$$

Because $\exp(-iky) = \cos(ky) - i\sin(ky)$, equation (18) can be simplified to obtain the cosine transform of the high-oscillation function integral about the Fourier transform:

$$h(x, k, z, t) = 2\int_0^{\infty} H(x, y, z, t)\, cos(ky) dy \tag{19}$$

The numerical filtering algorithm based on the Bessel and Cosine functions is used to solve (19), and the algorithm formula is

$$h(x, k, z, t) = (2\pi)^{1/2} c\, cos(n\Delta) \left[\sum_{n=-\infty}^{+\infty} f\left(e^{n\Delta}/k\right)\right] / k \tag{20}$$

Here, $\Delta = \ln(10)/20$ is the sampling interval, $c\cos(n\Delta)$ is the filter coefficient of Cosine transform, and k is the discrete wavenumber.

(20) is used to calculate the wave number field value assigned to formula (14) at the initial moments. Then, the finite-difference recursive calculations are performed in the wave number domain field.

IV. BOUNDARY CONDITIONS

For the boundary conditions, the main problem is the outer boundary for the whole-space model, i.e., the truncation boundary settings of the two-dimensional space in the wave number domain. In this study, based on the establishment principle of the unidirectional wave absorbing boundary conditions, the absorbing boundary conditions of the two-dimensional electromagnetic diffusion equation in the wave number domain are established. The second-order approximation on the boundary and its differential form are shown below.

The absorbing boundary condition of the second-order boundary finite-difference approximation of the $x = 0$ boundary is

$$\begin{aligned} h^{n+1}(i, 0) &= r\left(1/\Delta x - \lambda/2 - 1/2\lambda\Delta z^2\right) A_1 \\ &- r\left(1/\Delta x + \lambda/2 + 1/2\lambda\Delta z^2\right) A_2 \\ &+ \left(r/4\lambda\Delta z^2\right) A_3 - A_4 \end{aligned} \tag{21}$$

here

$$\begin{cases} r = 8\lambda\Delta t / (\mu\sigma) \\ A_1 = h^n(i, 1) \\ A_2 = h^n(i, 0) \\ A_3 = h^n(i+1, 1) + h^n(i+1, 0) \\ \qquad + h^n(i-1, 1) + h^n(i-1, 0) \\ A_4 = h^{n+1}(i, 1) + h^{n-1}(i, 1) + h^{n-1}(i, 0) \end{cases}$$

The absorbing boundary condition of the second-order boundary finite-difference approximation of the $x = h$ right boundary is

$$\begin{aligned} h^{n+1}(i, j) &= -r\left(1/\Delta x + \lambda/2 + 1/2\lambda\Delta z^2\right) A_1 \\ &+ r\left(1/\Delta x - \lambda/2 - 1/2\lambda\Delta z^2\right) A_2 \\ &+ \left(r/4\lambda\Delta z^2\right) A_3 - A_4 \end{aligned} \tag{22}$$

here

$$\begin{cases} r = 8\lambda\Delta t/(\mu\sigma) \\ A_1 = h^n(i,j) \\ A_2 = h^n(i,j-1) \\ A_3 = h^n(i+1,j-1) + h^n(i+1,j) \\ \quad + h^n(i-1,j-1) + h^n(i-1,j) \\ A_4 = h^{n+1}(i,j-1) + h^{n-1}(i,j-1) + h^{n-1}(i,j) \end{cases}$$

The absorbing boundary condition of the second-order boundary finite-difference approximation of the $z = 0$ boundary is

$$\begin{aligned} h^{n+1}(0,j) = {} & r\left(1/\Delta z - \lambda/2 - 1/2\lambda\Delta x^2\right)A_1 \\ & - r\left(1/\Delta z + \lambda/2 + 1/2\lambda\Delta x^2\right)A_2 \\ & + \left(r/4\lambda\Delta x^2\right)A_3 - A_4 \end{aligned} \tag{23}$$

here

$$\begin{cases} r = 8\lambda\Delta t/(\mu\sigma) \\ A_1 = h^n(1,j) \\ A_2 = h^n(0,j) \\ A_3 = h^n(1,j+1) + h^n(0,j+1) \\ \quad + h^n(1,j-1) + h^n(0,j-1) \\ A_4 = h^{n+1}(1,j) + h^{n-1}(1,j) + h^{n-1}(0,j) \end{cases}$$

The absorbing boundary condition of the second-order boundary finite-difference approximation of the $z = h$ boundary is

$$\begin{aligned} h^{n+1}(i,j) = {} & -r\left(1/\Delta z + \lambda/2 + 1/2\lambda\Delta x^2\right)A_1 \\ & + r\left(1/\Delta z - \lambda/2 - 1/2\lambda\Delta x^2\right)A_2 \\ & + \left(r/4\lambda\Delta x^2\right)A_3 - A_4 \end{aligned} \tag{24}$$

here

$$\begin{cases} r = 8\lambda\Delta t/(\mu\sigma) \\ A_1 = h^n(i,j) \\ A_2 = h^n(i-1,j) \\ A_3 = h^n(i-1,j+1) + h^n(i,j+1) \\ \quad + h^n(i-1,j-1) + h^n(i,j-1) \\ A_4 = h^{n+1}(i-1,j) + h^{n-1}(i-1,j) + h^{n-1}(i,j) \end{cases}$$

V. INVERSE FOURIER TRANSFORM ALGORITHM AND WAVE NUMBER SELECTION

A. INVERSE FOURIER TRANSFORM ALGORITHM

To obtain the (x, y, z) space transient field value, we must transform the wave number domain into the spatial domain through the inverse Fourier transform algorithm:

$$H(x,y,z,t) = \frac{2}{\pi}\int_0^{\infty} h(x,k,z,t)\cos(ky)\,dk \tag{25}$$

The inverse Fourier transform algorithm generally changes the integration interval 0-∞ into a limited range of $10^{-3} < k < 10$ based on the variation of $h(x, y, z)$ with changing k. A piecewise exponential function is used to fit the plot function in a limited range, and the integral value can be calculated by determining the integrand values of the endpoint of each segment to obtain the inverse Fourier integral. A large number of trial calculations show that the curve of transient electromagnetic field $h(x, y, z)$ with changing k first increases and subsequently decreases. In performing inverse Fourier Transform, this function curve will be divided into two large segments of increasing and decreasing. The inverse Fourier transform values can be finally obtained by superimposing with the positive exponential function fitting in the increasing segment and the negative exponential function fitting in the decreasing section. We calculated them as follows:

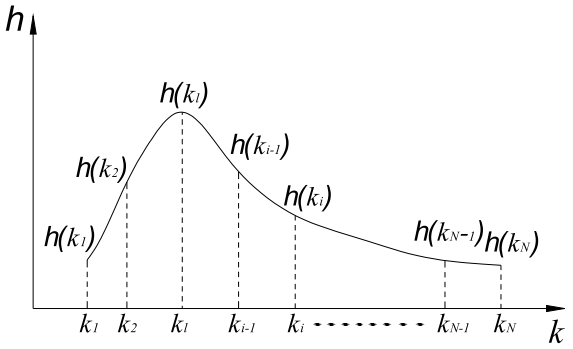

FIGURE 3. Sketch map for the fourier inverse transform.

The h value of each node at different moments are obtained by the finite-difference time domain in the wave number domain. In other words, for a node, N values of $h(x, k_1, z, t)$, $h(x, k_2, z, t), \ldots, h(x, k_N, z, t)$, etc. are known; the inverse Fourier integral interval is $k_1 \sim k_N$. Then, the integration interval is divided into $(N-1)$ subintervals; k of each known h value can be consider a sub-interval endpoint. Then, the intervals are $(k_1, k_2), (k_2, k_3), \ldots, (k_{N-1}, k_N)$, as shown in Figure 3. The integrand function h in any sub-interval is approximated by the exponential function, i.e., the integration of the subinterval is

$$\begin{aligned} & \int_{k_i}^{k_{i+1}} A_i \exp(a_i k)\cos(ky)\,dk \\ & = A_i\left(a_i^2 + y^2\right)^{-1} \cdot \exp(a_i k)\left[y\sin(ky) - a_i\cos(ky)\right]\Big|_{k_i}^{k_{i+1}} \\ & \qquad (i = 1, \cdots\cdots N-1), \end{aligned}$$

a_i is the i filter coefficient.

For the nodes in the main cross section, which is through the source and perpendicular to the trend of the geological body, we can set $y = 0$. Then, the above equation is simplified to

$$\int_{k_i}^{k_{i+1}} A_i \exp(a_i k)\cos(ky)\,dk = [h(k_i) - h(k_{i+1})]/a_i$$

For the nodes in other cross sections, $y \neq 0$, and the equation above is

$$\int_{k_i}^{k_{i+1}} A_i \exp(a_i k)\cos(ky)\,dk = \left(a_i^2 + y^2\right)^{-1} \{h(k_{i+1})[y\sin(k_{i+1}y) - a_i\cos(k_{i+1}y)] - h(k_i)[y\sin(k_i y) - a_i\cos(k_i y)]\}$$

The integral values of all sub-intervals are summed, and the inverse Fourier transform value of (25) is obtained.

B. WAVE NUMBER k SELECTION

The selection of wave number k significantly affects the computational accuracy and computing time. Thus, we drew the wave number selection method of Luo Yanzhong [24] on an electrical point source [25]–[27]. The maximum and minimum distances [28], [29] between the transmitter and the receiver are $r_{\max}$ and $r_{\min}$, so the minimum and maximum of wave number are selected by

$$\begin{cases} k_1 = 0.1/r_{max} \\ k_N = 3/r_{min} \end{cases}$$

Number N of wave numbers is calculated as follows

$$N = (lnk_N - lnk_1)/ln\alpha + 1$$

If the calculated N is not equal to an integer, only an integer number can involve through rounding. According to the trial experience, it is proper when α is 2.5. Of course, α should be slightly adjusted in some special conditions. Various trials show that it is sufficient when N is 10. If N exceeds 10, the accuracy of the calculation did not significantly improve, but the calculating time increased. k should be 10^{-5} - 10^{-1} with the equal logarithm interval.

VI. RESULTS AND ANALYSIS

To verify the effectiveness of the algorithm, the algorithm was first tested with the theoretical model of a uniform whole-space with the analytical solutions. Then, it is used to calculate and analyze the geoelectric model of the special collapse columns in the process of coal mine roadway drivage.

A. UNIFORM WHOLE-SPACE GEOELECTRIC MODEL

The electromagnetic field value is computed using the uniform whole-space geoelectric model with the resistance of 100 Ωm. The model length in the y direction is 200 m with an 81 × 81 space grid, and the grid interval is 10 m. In the model, according to (14), the maximum time interval is $\Delta t_{\max} \leq 0.314\mu s$, and the progressive manner with a variable time interval is used. The time interval and corresponding iterations are shown in Table 1. The number of k is 10, which is distributed at equal logarithmic intervals between 10^{-5} and 10^{-2}. The excitation source is located in the center of the grid space, and the excitation direction points to the x-direction. The observation station is 100 m from the excitation source. The duration of the simulated transient

TABLE 1. Time-step size and number of steps.

	1	2	3	4	5
Time-step (μs)	1e-2	4e-2	1e-1	2e-1	3e-1
Number of step	8000	8000	8000	8000	8000

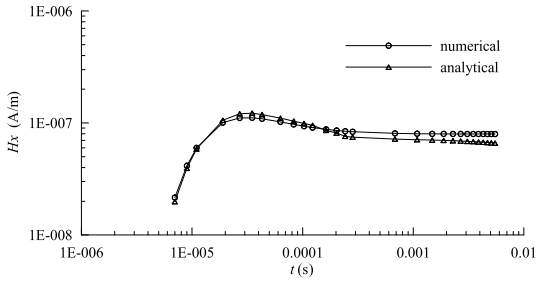

FIGURE 4. Comparison between the calculated values by the numerical and analytical methods.

electromagnetic diffusion was 5.88 ms, and the calculation took approximately 20 s to complete on a CPU2.13-GHz, 1G memory computer.

Figure 4 shows the comparison of the x-direction component of magnetic field Hx between numerical and analytical results. The numerical results are consistent with the analytical results, and the relative error is less than 5%.

B. COLLAPSE COLUMN MODEL

The collapse-column model is shown in Fig. 5. There are five layers in this model with a height of 400 m, and each layer is 80 m thick. The electrical parameters from top to bottom have layer resistivities of 500 Ωm, 50 Ωm, 100 Ωm, 50 Ωm and 500 Ωm. The collapse column is 240 m high, the diameter is 40 m, the resistivity is 1 Ωm, and the vertical distance from the excitation source is 40 m. The excitation source is placed in the third layer in the geometric center of the model and parallel to the bedding.

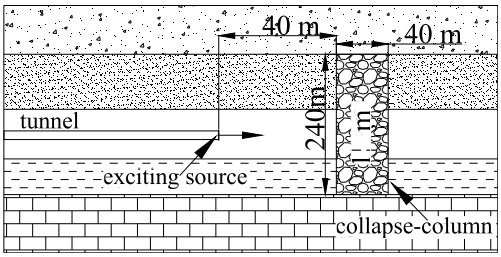

FIGURE 5. Collapse-column model.

Figure 6 shows the contours of the transient electrical field (unit: V/m) of the low-resistivity collapse column at each time. In the initial transient electromagnetic induction time (Fig. 6-a, 9 μs), the transient electric field was mainly distributed near the source, the outer edge of the transient

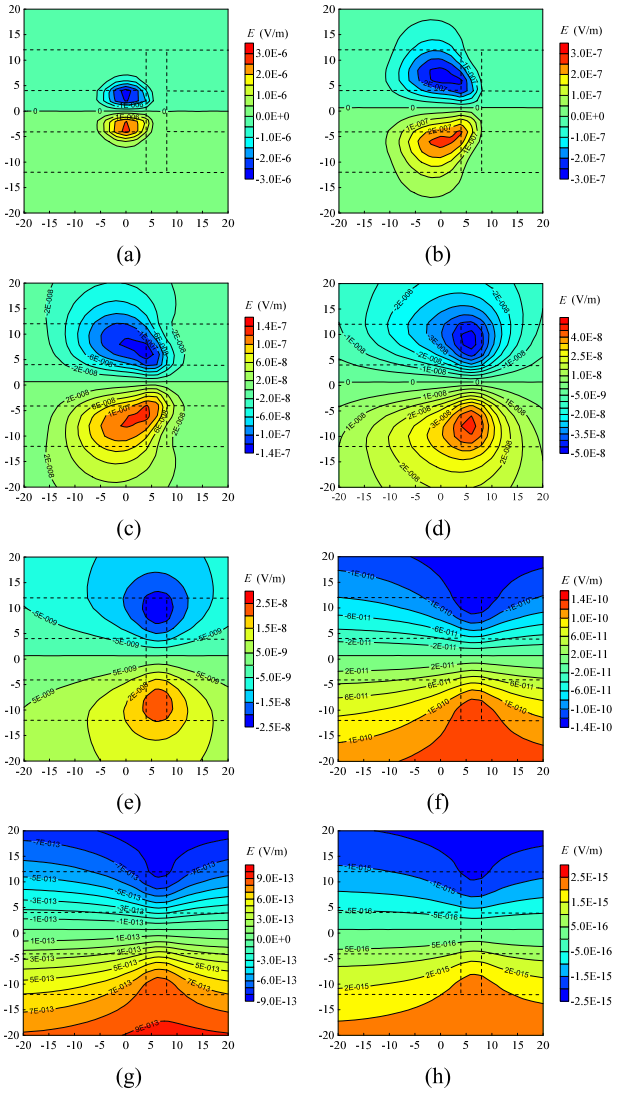

FIGURE 6. Transient electromagnetic contour. Panels (a-h) are the E value for the delay times 9 μs, 43 μs, 83 μs, 203 μs, 683 μs, 1883 μs, 3483 μs and 5883 μs, respectively.

electric field only spread to the collapse column, and the induced current density center was in the plane of the excitation source and perpendicular to the bedding plane. With time (Figs. 6-b and 6-c, 43-83 μs), the induced current density center stretched along the direction of bedding and gradually moved to the internal collapse column, and the collapse column began to affect the temporal and spatial distribution of the electric field (Figs. 6-d and 6-e, 203-683 μs). With more time (1883 μs -), the induced current density center completely moved into the collapse column and diffused upward and downward along the direction perpendicular to the bedding until the decay vanished (Figs. 6-f-6-h). The results show that only the low-resistivity collapse column changed the normal diffusion of the transient electromagnetic field in the layered space. When the induced current density center fully moved inside the collapse column, the collapse column becomes a ''secondary source'' to radiate electromagnetic fields to the entire space, and the observed signals mainly reflect the attenuation information of the transient electromagnetic field under the effect of the collapse column. On this account, the advanced detection with the TEM in the roadway of coal mines can well reflect the abnormality of the water-conducting collapse column in front of the tunnel face.

VII. CONCLUSIONS

The 2.5D finite-difference time domain algorithm only simulates the diffusion of the whole-space transient electromagnetic field excited by a magnetic dipole in the 2D geoelectric model. Compared with the 3D numerical simulation, the calculation speed is high, and the calculation cost is low. The difficulty of this algorithm is that the 3D source is transformed from a 3D space domain to a 2D wave number domain by the Fourier transform, and the calculated results are transformed back to the space domain by the inverse Fourier transform after the difference calculation. The digital filter method in the transform and the number and value of k affect the accuracy of the calculation. The time interval affects the accuracy and speed of the calculation. The time interval is related to the mesh and wave number in the wave number domain. The maximum time interval is adjusted considering the stability of the calculation. According to the variation in the whole-space transient electromagnetic field $h(x, k, z)$ with changing k, the sub-fitting exponential function is used in the inverse Fourier transform to ensure the reliability of the calculation. The comparison between the simulation result and the analytical solution of the whole-space uniform model verified the correctness of the algorithm. The simulation results of a water-bearing collapse column show that the transient electric field distribution is consistent with the electromagnetic field diffusion law and that the low-resistance collapse column is well reflected.

DECLARATION OF INTEREST

The authors declare that there is no conflict of interests regarding the publication of this paper.

REFERENCES

[1] W. Y. Hu and G. Tian, ''Mine water disaster type and prevention and control countermeasures in China,'' (in Chinese), *Coal Sci. Technol.*, vol. 38, no. 1, pp. 92–96, Jan. 2010.

[2] S.-C. Liu, Z.-X. Liu, and Z.-H. Jang, ''Application of TEM in hydrogeological prospecting of mining district,'' *J.-China Univ. Mining Technol.-Chin. Ed.*, vol. 34, no. 4, pp. 414–417, Apr. 2005.

[3] J.-C. Yu, Z.-X. Liu, and J.-Y. Tang, ''Research on full space transient electromagnetism technique for detecting aqueous structures in coal mines,'' *J. China Univ. Mining Technol.*, vol. 17, no. 1, pp. 58–62, Mar. 2007.

[4] J.-C. Yu, Z.-X. Liu, J.-Y. Tang, and Y.-Z. Wang, ''Transient electromagnetic detecting technique for water hazard to the roof of fully mechanized sub-level caving face,'' *J.-China Univ. Mining Technol.-Chin. Ed.*, vol. 36, no. 4, pp. 542–546, Apr. 2007.

[5] Z.-H. Jiang, J.-H. Yue, and S.-C. Liu, ''Prediction technology of buried water-bearing structures in coal mines using transient electromagnetic method,'' *J. China Univ. Mining Technol.*, vol. 17, no. 2, pp. 164–167, Jun. 2007.

[6] G. Q. Xue, Y. Yan, X. Li, and Q. Y. Di, ''Transient electromagnetic S-inversion in tunnel prediction,'' *Geophys. Res. Lett.*, vol. 34, no. 18, pp. 995–1005, Sep. 2007, doi: 10.1029/2007GL031080.

[7] G. Q. Xue and X. Li, "The technology of TEM tunnel prediction imaging," (in Chinese), *Chin. J. Geophys.*, vol. 51, no. 3, pp. 894–900, May 2008.
[8] H. F. Sun, X. Li, S. C. Li, Z. P. Qi, M. X. Su, and Y. Xue, "Multi-component and multi-array TEM detection in karst tunnels," *J. Geophys. Eng.*, vol. 9, no. 4, pp. 359–373, Jul. 2012.
[9] J.-C. Yu, Y.-Z. Wang, J. Liu, and X.-B. Zeng, "Time-depth conversion of transient electromagnetic method used in coal mines," *J. China Univ. Mining Technol.*, vol. 18, no. 5, pp. 46–50, Dec. 2008. [Online]. Available: https://doi.org/10.1016/S1006-1266(08)60291-6
[10] H. Y. Yang, D. Juzhi, Z. Hua, and Y. Jian-Hua, "Research on full-space apparent resistivity interpretation technique in mine transient electromagnetic method," (in Chinese), *Chin. J. Geophys.*, vol. 53, no. 3, pp. 651–656, 2010.
[11] Z. Qi, Q. Zhi, X. Li, and H. Sun, "Full-field apparent resistivity definition of underground transient electromagnetic data," (in Chinese), *Chin. J. Rock Mech. Eng.*, vol. 34, no. 10, pp. 1–9, 2015, doi: 10.13722/j.cnki.jrme.2014.1310.
[12] M.-X. Su, S.-C. Li, Y.-G. Xue, X. Li, and D.-H. Qiu, "TEM apparent longitudinal conductance interpretation in tunnel geological forecast," (in Chinese), *Chin. J. Geotechn. Eng.*, vol. 11, pp. 16–25, Nov. 2010.
[13] J. Cheng, F. Li, S. Peng, X. Sun, J. Zheng, and J. Jia, "Joint inversion of TEM and DC in roadway advanced detection based on particle swarm optimization," *J. Appl. Geophys.*, vol. 12, no. 3, pp. 30–35, Dec. 2015. [Online]. Available: https://doi.org/10.1016/j.jappgeo.2015.09.008
[14] J.-L. Cheng, D. Chen, G.-Q. Xue, H. Qiu, and X.-T. Zhou, "Synthetic aperture imaging in advanced detection of roadway using mine transient electromagnetic method," (in Chinese), *Chin. J. Geophys.*, vol. 59, no. 2, pp. 190–198, Mar. 2016, doi: 10.1002/cjg2.20225.
[15] S. Krivochieva and M. Chouteau, "Whole-space modeling of a layered earth in time-domain electromagnetic measurements," *J. Appl. Geophys.*, vol. 50, no. 4, pp. 375–391, Jul. 2002. [Online]. Available: https://doi.org/10.1016/S0926-9851(02)00164-7
[16] J. H. Yue, H. Y. Yang, and B. Hu, "3D finite difference time domain numerical simulation for TEM in-mine," (in Chinese), *Prog. Geophys.*, vol. 22, no. 6, pp. 1904–1909, 2007.
[17] J. H. Yue and H. Y. Yang, "Research on response of transient electromagnetic field in underground mine with boundary condition of laneway," *J.-China Univ. Mining Technol.-Chin. Ed.*, vol. 37, no. 2, pp. 152–156, Feb. 2008.
[18] E. V. Onegova and M. I. Epov, "3D simulation of transient electromagnetic field for geosteering horizontal wells," *Russian Geol. Geophys.*, vol. 52, no. 7, pp. 725–729, Jul. 2011. [Online]. Available: https://doi.org/10.1016/j.rgg.2011.06.005
[19] S. Li, H. Sun, X. Lu, and X. Li, "Three-dimensional modeling of transient electromagnetic responses of water-bearing structures in front of a tunnel face," *J. Environ. Eng. Geophys.*, vol. 19, no. 1, pp. 13–32, Mar. 2014. [Online]. Available: https://doi.org/10.2113/JEEG19.1.13
[20] S. Yan, M. S. Chen, and J. M. Fu, "Direct time-domain numerical analysis for transient electromagnetic fields," (in Chinese), *Chin. J. Geophys.*, vol. 45, pp. 277–287, Mar. 2002, doi: 10.1002/cjg2.240.
[21] M. L. Oristaglic and G. W. Hohmann, "Diffusion of electromagnetic fields into a two-dimensional earth: A finite-difference approach," *Geophysics*, vol. 49, no. 7, pp. 870–894, Jul. 1984. [Online]. Available: https://doi.org/10.1190/1.1441733
[22] N. M. Nabigian, "Electromagnetic methods," (in Chinese), in *Applied Geophysics*, vol. 1, J. X. Zhao and Y. J. Wang, Eds. Beijing, China: Geological Publishing House, 1992.
[23] H. J. Wang, "Digital filter algorithm of the sine and cosine transform," (in Chinese), *Chin. J. Eng. Geophys.*, vol. 1, no. 4, pp. 329–335, Apr. 2004.
[24] Y. Z. Luo and Y. L. Meng, "Some problems on resistivity modeling for two-dimensional structures by the finite-element method," (in Chinese), *Chin. J. Geophys.*, vol. 29, no. 6, pp. 613–621, 1986.
[25] S. Jie, Z. Weisong, J. Xiangjun, and Z. Xin, "Underwater broadband acoustic scattering modelling based on FDTD," *Electronics*, vol. 21, no. 2, pp. 58–64, 2015.
[26] J. Yu, R. Malekian, J. Chang, and B. Su, "Modeling of whole-space transient electromagnetic responses based on FDTD and its application in the mining industry," *IEEE Trans. Ind. Informat.*, to be published.
[27] X. Jin, J. Shao, X. Zhang, W. An, and R. Malekian, "Modeling of nonlinear system based on deep learning framework," *Nonlinear Dyn.*, vol. 84, no. 3, pp. 1327–1340, 2016.
[28] Z. Xin, S. Jie, A. Wenwei, Y. Tiantian, and R. Malekian, "An improved time-frequency representation based on nonlinear mode decomposition and adaptive optimal kernel," *Electronics*, vol. 22, no. 4, pp. 52–57, 2016.
[29] S. Hao, S. Wang, R. Malekian, B. Zhang, W. Liu, and Z. Li, "A geometry surveying model and instrument of a scraper conveyor in unmanned longwall mining faces," *IEEE Access*, vol. 5, pp. 4095–4103, 2017.

ZHIHAI JIANG received the Ph.D. degree from the Department of Applied Geophysics, China University of Mining and Technology, China, in 2008. He is currently an Associate Professor with the China University of Mining and Technology, China. His research interest is mine geophysics.

SHUCAI LIU received the Ph.D. degree from the Department of Applied Geophysics, China University of Mining and Technology, China, in 2007. He is currently a Professor with the China University of Mining and Technology, China. His research interest is mine geophysics.

REZA MALEKIAN (M'10–SM'17) is currently an Associate Professor and Research Group Head in advanced sensor networks with the Department of Electrical, Electronic, and Computer Engineering, University of Pretoria, Pretoria, South Africa. His current research interests include advanced sensor networks, Internet of Things, and mobile communications. He is also a Chartered Engineer and a Professional Member of the British Computer Society. He is an Associate Editor for the IEEE INTERNET of THINGS Journal.